GEOPHYSICS, VOL. 79, NO. 3 (MAY-JUNE 2014); P. V107–V114, 10 FIGS.
10.1190/GEO2013-0206.1

Absorption-compensation method by l_1-norm regularization

Shoudong Wang[1] and Xiaohong Chen[1]

ABSTRACT

Absorption in subsurface media greatly reduces the resolution of seismic data. Absorption not only dissipates the high-frequency components of the wave, but it also distorts the seismic wavelet. The inverse Q-filtering method is an effective method to correct the attenuation and dispersion of the seismic wave. We evaluated an absorption compensation method based on l_1-norm regularization. Forward modeling in the absorption medium is described by a Fredholm integral equation in the time domain, and the absorption compensation comes down to solving the Fredholm integral equation. The solutions of the Fredholm integral equation are extremely unstable. Generally, l_2-norm regularization can be used to seek stable solutions of the Fredholm integral equation, but it makes the solutions smooth and reduces the resolution of seismic data. We used l_1-norm regularization to overcome instability of solving the integral equation; it makes the solutions have a higher resolution than l_2-norm regularization. The iteratively reweighted method is used to solve the minimization problem. Tests on synthetic and real data examples showed that the absorption compensation method that we evaluated can effectively correct the attenuation and dispersion of the seismic wave.

INTRODUCTION

The subsurface medium is not completely elastic, and it has viscosity. When the seismic wave propagates in a subsurface medium, high-frequency component attenuation and speed dispersion will occur. The absorption limits the resolution of seismic data, distorts the seismic wavelet, and therefore affects the correct interpretation of seismic data. The absorbing effect of the stratum medium on the seismic wave can be described by the Q model, and a more well-known model is the Futterman model (Varela et al., 1993). Toverud and Ursin (2005) compares eight kinds of attenuation models using VSP seismic data and concludes that the Futterman model can better describe the seismic wave propagation law in subsurface media.

To eliminate the influence of the absorption and improve the resolution of seismic data, attenuation of seismic data must be corrected. The correction includes the amplitude correction and velocity dispersion correction. In general, dispersion correction is stable and amplitude correction is unstable. Bickel and Natarajan (1985) propose Q deconvolution, which compensates attenuation by filtering the observed trace with the forward time-varying filter with Q replaced by $-Q$. Hargreaves and Calvert (1991) give an inverse Q-filter method in the frequency domain. In this method, the attenuation role of the medium is seen as a Q-filter and the inverse Q-filter is seen as wavefield back-propagation. The phase distortion can be better corrected by the method, and amplitude correction is ignored to avoid instability. Hargreaves (1992) and Bickel (1993) show an inverse Q-filter method based on the Pareto-Levy stretch, which can better deal with the instability of amplitude compensation. Wang (2002, 2003, 2006) gives an inverse Q-filter method based on the wavefield continuation theory, which can do the amplitude compensation and phase correction simultaneously. The amplitude limit compensation method is used to solve the instability of amplitude compensation. For the multilayer case, the compensation of absorption and attenuation is achieved with a layer-by-layer application of the method. Zhang and Ulrych (2007) formulates the compensation of absorption and attenuation as a least-squares problem and imposed regularization by means of Bayes's theorem. Qaji and Rietbrock (2011) present a technique for compensating for the effects of energy dissipation and velocity dispersion in seismic-wave propagating in viscoacoustic earth media. Replacing wavenumbers with slownesses in the calculation of exponential functions circumvents the undesirable effects of instability at high frequencies and traveltime. Baan (2012) gives a procedure for combined dispersion and attenuation correction, which comprises first applying dispersion corrections using phase-only inverse Q filtering, followed by zero-phase time-varying Wiener deconvolution. Margrave et al. (2011) describe Gabor deconvolution, which combines the essential ideas of stationary deconvolution and inverse Q filtering and can

Manuscript received by the Editor 4 June 2013; revised manuscript received 4 January 2014; published online 2 May 2014.
[1]China University of Petroleum, State Key Laboratory of Petroleum Resource and Prospecting, National Engineering Laboratory for Offshore Oil Exploration, Beijing, China. E-mail: ctlab@cup.edu.cn; chenxh@cup.edu.cn.

correct for wavelet shape and attenuation. Innanen and Lira (2010) derive an inverse-scattering Q-compensation procedure that operates in the absence of prior knowledge of the properties of the subsurface, including its Q structure. Mittet et al. (1995), Song and Innanen (2002), and Mittet (2007) discuss the compensation method in the migration process.

Shou-Dong (2011) describes the attenuation compensation problem as an inversion problem of the Fredholm integral equation in the frequency domain and uses the Tikhonov regularization to improve inversion stability. In the regularization, the l_2-norm is used. In this paper, the attenuation compensation is also formulated as the inversion problem of the Fredholm integral equation, but in the time domain. We discuss the weighted inversion and the l_1-norm regularization. The l_1-norm regularization is more robust to noise data and can achieve higher resolution. The iteratively reweighted method is used to solve the l_1-norm minimization problem. Synthetic and real examples demonstrate the effectiveness of the presented method.

FORWARD MODELING

Propagation of seismic wave in attenuation medium

The propagation of a seismic wave in an attenuation medium has been discussed by many authors. Futterman (1962), Azimi et al. (1968), and Kjartansson (1979) all discuss the problem. In this paper, we use the Futterman model. Considering that the attenuation of each frequency is different, we first discuss the harmonic wave. Suppose that there is a time signal at the z position and its angular frequency is ω, denoted by $P(z,\omega,t)$. After propagating distance Δz, the wave can be written as

$$P(z+\Delta z,\omega,t)=P(z,\omega,t)\exp(ik_z\Delta z), \tag{1}$$

where ω is the time angular frequency and k_z is the spatial angular frequency. If the medium is completely elastic,

$$k_z=-\left(\frac{\omega}{v}\right), \tag{2}$$

where v is the velocity. To introduce the attenuation in medium, the complex velocity is used in this model, as described by Wang (2002). Replace the velocity in formula 2 with the complex velocity,

$$\frac{1}{v(z)}=\frac{1}{v(z,\omega)}\left(1-\frac{i}{2Q(z)}\right), \tag{3}$$

where $v(z,\omega)$ is the frequency-dependent phase velocity and $Q(z)$ is the medium quality factor. We use a model for the phase velocity $v(z,\omega)$ defined by

$$v(z,\omega)=v(z,\omega_0)\left|\frac{\omega}{\omega_0}\right|^{\gamma}, \tag{4}$$

where

$$\gamma=\frac{2}{\pi}\tan^{-1}\left(\frac{1}{2Q}\right)\approx\frac{1}{\pi Q} \tag{5}$$

and $v(z,\omega_0)$ is the reference velocity, which generally is the phase velocity at dominant frequency ω_0. Combining formulas 1–4, we get

$$P(z+\Delta z,\omega,t)=P(z,\omega,t)\exp\left(-i\omega\frac{\Delta z}{v(z,\omega_0)}\left|\frac{\omega_0}{\omega}\right|^{\gamma}\left(1-\frac{i}{2Q(z)}\right)\right). \tag{6}$$

Equation 6 is the law of harmonic wave propagation in an attenuation medium. For the seismic wave, we can analyze it by the Fourier transform.

Forward modeling in an attenuation medium

In an elastic medium, it is well known, that the formula for making a poststack seismic record is the convolution model:

$$s(t)=r(t)*w(t) \tag{7a}$$

or

$$s(t)=\int r(\tau)w(t-\tau)\mathrm{d}\tau, \tag{7b}$$

where t and τ are the traveltime, $s(t)$ is the seismogram, $r(t)$ is the reflection coefficient, and $w(t)$ is the wavelet. In the elastic medium, the wavelet is constant, but in the attenuation medium, the wavelet is changing. The wavelet is represented by $w(\tau,t)$, where τ is the two-way traveltime. Therefore, the convolution model with the time-varying wavelet changes to

$$s(t)=\int w(\tau,t)r(\tau)\mathrm{d}\tau, \tag{8}$$

where the wavelet $w(\tau,t)$; can be derived from formula 6. Assume that $w(0,t)=w(t)$.

The relationship between the wavelet and its frequency spectrum is

$$w(t)=\int_{-\infty}^{\infty}\hat{w}(\omega)e^{i\omega t}\mathrm{d}\omega. \tag{9}$$

Equation 9 shows that $w(t)$ can be decomposed into a series of simple harmonic waves $\hat{w}(\omega)e^{i\omega t}$. According to equation 6, the attenuated harmonic wave at z, which propagates from the surface to depth z and reflects back to the surface, can be written as

$$\hat{w}(\omega)e^{i\omega t}\exp\left(-i\omega\frac{2z}{v(z,\omega_0)}\left|\frac{\omega_0}{\omega}\right|^{\gamma}\left(1-\frac{i}{2Q(z)}\right)\right). \tag{10}$$

Replacing the depth z with the two-way traveltime τ, formula 10 can be rewritten as

$$\hat{w}(\omega)e^{i\omega t}\exp\left(-i\omega\tau\left|\frac{\omega_0}{\omega}\right|^{\gamma}\left(1-\frac{i}{2Q(\tau)}\right)\right). \tag{11}$$

Taking the integral with respect to frequency, the attenuated wavelet at τ can be obtained:

$$w(\tau,t)=\int_{-\infty}^{\infty}\hat{w}(\omega)\exp\left(-i\omega\tau\left|\frac{\omega_0}{\omega}\right|^{\gamma}\left(1-\frac{i}{2Q(\tau)}\right)\right)e^{i\omega t}\mathrm{d}\omega. \tag{12}$$

Now the seismogram can be made by formulas 8 and 12. Equation 8 is a standard first kind of Fredholm integral equation. The compensation problem is how to compute the reflection coefficient from the seismogram. The compensation algorithm can be realized by solving the Fredholm integral equation.

COMPENSATION METHOD

Assuming that the deconvolution has been done on the seismic records and the wavelet is eliminated, formula 12 can be rewritten as

$$w(\tau,t)=\int_{-\infty}^{\infty}\exp\left(-i\omega\tau\left|\frac{\omega_0}{\omega}\right|^{\gamma}\left(1-\frac{i}{2Q(\tau)}\right)\right)e^{i\omega t}d\omega. \quad (13)$$

Equation 13 is the integral kernel function. In mathematics, the Fredholm integral equation is a branch of the inverse problem and its numerical solution is often unstable. Stability measures must be taken to get a stable solution. A more effective stabilization method is Tikhonov regularization, which is a well-known method for solving ill-posed problem. There is much research on this method, and its basic idea is to construct a stabilizing functional. The problem of solving integral equation 8 can be reduced to the minimization problem of the functional:

$$\mathrm{OBJ}=\left\|\int_{-\infty}^{\infty}w(\tau,t)r(\tau)d\tau-s(t)\right\|^2. \quad (14)$$

The solving process of minimizing functional 14 is unstable. The Tikhonov regularization method is to add the stability functional to functional 14. We construct the objective functional,

$$\mathrm{OBJ}=\left\|\int_{-\infty}^{\infty}w(\tau,t)r(\tau)d\tau-s(t)\right\|^2+\beta\Omega(r(t')), \quad (15)$$

where $\beta>0$ is the regularization parameter, $\Omega(r(t'))$ is the stabilizing functional, which can be

$$\Omega(r(t'))=\int_{-\infty}^{\infty}(r(t'))^2\mathrm{d}t', \quad (16)$$

$$\Omega(r(t'))=\int_{-\infty}^{\infty}\left(\frac{dr(t')}{dt'}\right)^2\mathrm{d}t', \quad (17)$$

or

$$\Omega(r(t'))=\int_{-\infty}^{\infty}\left(\frac{d^2r(t')}{d(t')^2}\right)^2\mathrm{d}t'. \quad (18)$$

These functionals are three kinds of measures of the reflection coefficient. They are, respectively, the function itself, the first derivative of the function, and the second derivative. The different stabilizing items have different assumptions on the reflection coefficient. To get a higher resolution numerical solution, the l_1-norm regularization method can also be used and

$$\Omega(r(t'))=\int_{-\infty}^{\infty}|r(t')|\mathrm{d}t'. \quad (19)$$

The reflection coefficient $r(t')$ can be solved through minimizing functional 15 by a numerical method, and the compensation can be achieved.

The l_2-norm regularization numerical method

The above compensation method is discussed in the continuous space. Now, we discuss its numerical solving method. The discrete form of equation 8 is

$$\mathbf{WR}=\mathbf{S}, \quad (20)$$

where $\mathbf{W}$, $\mathbf{R}$, and $\mathbf{S}$ are the integral kernel matrix, reflection coefficient vector, and seismic record vector, respectively. The objective function 14 can be rewritten as

$$\mathrm{OBJ}=\|\mathbf{WR}-\mathbf{S}\|^2. \quad (21)$$

Because $\Omega(r(t'))$ is one of the formulas (equations 16–18), the objective functional (equation 15) can be rewritten as

$$\mathrm{OBJ}=\|\mathbf{WR}-\mathbf{S}\|^2+\beta\|\mathbf{\Omega R}\|^2, \quad (22)$$

where $\mathbf{\Omega}$ is the matrix corresponding to equations 16–18. To minimize formula 22, the reflection coefficient $\mathbf{R}$ can be obtained:

$$\mathbf{R}=(\mathbf{W^TW}+\boldsymbol{\beta}\mathbf{\Omega^T\Omega})^{-1}\mathbf{W^TS}. \quad (23)$$

Formula 23 can be used to achieve the attenuation compensation.

Several numerical simulation examples are done to discuss the characteristics of each method. Figure 1 shows a reflection coefficient sequence. Figure 2 shows the synthetic seismic record and attenuation compensation results. Figure 2a shows five synthetic traces with different constant Q values ($Q=400,200,100,50,25$) using formulas 8 and 12. In the synthetic process, the Ricker wavelet with a dominant frequency of 50 Hz is used. As the Q value decreases, the more the seismic wave attenuates. Figure 2b–2d is the attenuation compensation results using formula 23, corresponding to formulas 16–18. The result shows that three stabilizing methods can correctly compensate the amplitude and phase for $Q=400$, 200, 100, 50. For $Q=25$, there is a slight difference in the three results. The contrast shows that the second-order stabilizing method has higher precision.

The weighted inversion

Figure 2a also shows that the value at the shallow position is large and at the deeper position, it is small. In functional 14, the deep value affects it less. To balance the effect to the functional, a weight function should be introduced in functional 14, which will improve the precision of the inversion method. Functional 14 can be rewritten as

$$\mathrm{OBJ}=\left\|\int_{-\infty}^{\infty}a(t)w(\tau,t)r(\tau)d\tau-a(t)s(t)\right\|^2, \quad (24)$$

where $a(t)$ is the weight function, which is an increase function with the increase of time, such as

$$a(t) = \exp\left(\frac{24\pi t}{Q}\right). \tag{25}$$

Formula 23 also can be used to minimize functional 24. Figure 3 is the same as Figure 2, but the weight function 25 is involved. Figure 3a is the synthetic record after applying weight function 25. Figure 3b–3d is the attenuation compensation results.

Comparing Figures 3b and 2b, 3c and 2c, and 3d and 2d, we can see that the weight function method can significantly improve the precision of the inversion results, specifically for $Q = 25$.

The above example is done using a wavelet with the dominant frequency of 50 Hz. Now, we do another test with the dominant frequency of 80 Hz. Figure 4a is the synthetic seismic record, and $Q = 25$ is used. The compensation result is displayed in Figure 4b, and the second-order stabilizing method is used. The result shows that the deep data are not recovered perfectly for the dominant frequency of 80 Hz and $Q = 25$. This demonstrates that the above method cannot recover data perfectly for the high-frequency data and small Q value. To recover high-frequency data, the l_1-norm regularization can be used.

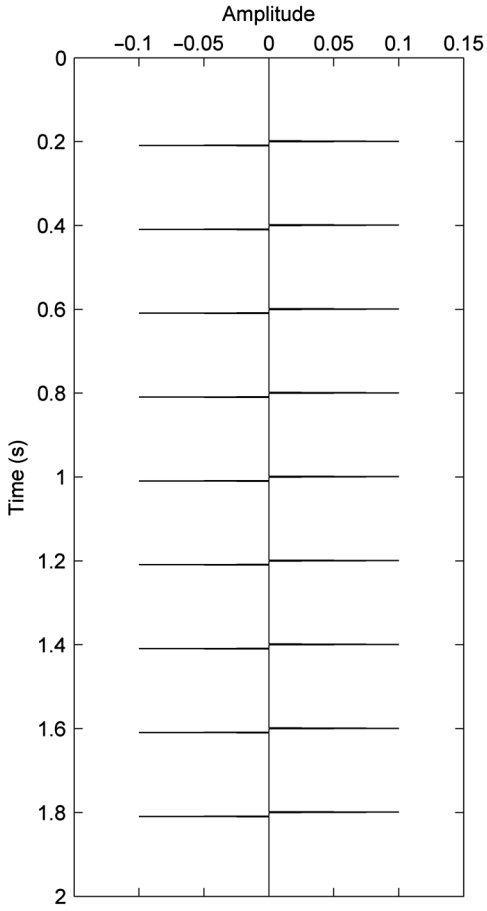

Figure 1. The reflection coefficient sequence.

The l_1-norm regularization numerical method

If the l_1-norm regularization method (equation 19) is used, then functional 24 becomes

$$OBJ = \| \int_{-\infty}^{\infty} a(t)w(\tau,t)r(\tau)d\tau - a(t)s(t)\|^2 + \beta \int_{-\infty}^{\infty} |r(t')|dt' \tag{26}$$

and the discrete form is

$$\text{OBJ} = \|\mathbf{AWR} - \mathbf{AS}\|^2 + \beta \sum_{i=1}^{n} |r_i|, \tag{27}$$

where r_i is the ith element of R. The l_1-norm imposes the sparseness as carried out by Zhang and Ulrych (2007). They impose the regularization by means of Bayes' theorem. They postulate that the reflectivity satisfies the Cauchy distribution and the regularization function is different from formula 27. Formula 27 is more difficult to minimize than formula 22 because the derivative of $\sum_{i=1}^{n} |r_i|$ is nonlinear. There is much research on the l_1-norm minimization. The iteratively reweighted method (Farquharson and Oldenburg, 1998) is used in this paper. For the case of $r_i = 0$, the objective function $\sum_{i=1}^{n} |r_i|$ needs to be modified to avoid discontinuity in its derivative. Thus, a small user-specified value ε is added to introduce stability if $r_i = 0$, and the modified objective function is then expressed as

$$\text{OBJ} = \|\mathbf{AWR} - \mathbf{AS}\|^2 + \beta \sum_{i=1}^{n} \sqrt{r_i^2 + \varepsilon^2}\,. \tag{28}$$

Because $\sum_{i=1}^{n} \sqrt{r_i^2 + \varepsilon^2}$ is the nonlinear function, the iterative method must be used. We follow the standard procedure of differentiating formula 28 with respect to r_i and equating the resulting equations to zero:

$$\mathbf{W}^T\mathbf{A}^T(\mathbf{AWR} - \mathbf{AS}) + \beta\mathbf{\Omega R} = 0, \tag{29}$$

where $\mathbf{\Omega}$ is the diagonal matrix given by

$$\mathbf{\Omega} = \text{diag}\left\{\frac{1}{\sqrt{(r_1)^2 + \varepsilon^2}}, \ldots, \frac{1}{\sqrt{(r_n)^2 + \varepsilon^2}}\right\}. \tag{30}$$

Suppose that we have an approximate solution r_i^k or the vector $\mathbf{R}^k$. Now we discuss how to get a new solution $\mathbf{R}^{k+1}$. Equation 29 can be written as

$$\mathbf{W}^T\mathbf{A}^T(\mathbf{AWR}^{k+1} - \mathbf{AS}) + \beta\mathbf{\Omega}^{k+1}\mathbf{R}^{k+1} = 0. \tag{31}$$

Because $\mathbf{\Omega}^{k+1}$ is a function of unknown parameter $\mathbf{R}^{k+1}$, this is a nonlinear system, and the iterative approach must be used. Make the approximation $\mathbf{\Omega}^{k+1} = \mathbf{\Omega}^k$, thus equation 31 becomes

$$\mathbf{W}^T\mathbf{A}^T(\mathbf{AWR}^{k+1} - \mathbf{AS}) + \beta\mathbf{\Omega}^k\mathbf{R}^{k+1} = 0. \tag{32}$$

This equation is easy to solve, and we can obtain the iterative formula,

$$\mathbf{R}^{k+1} = (\mathbf{W}^T\mathbf{A}^T\mathbf{A}\mathbf{W} + \beta\boldsymbol{\Omega}^k)^{-1}\mathbf{W}^T\mathbf{A}^T\mathbf{A}\mathbf{S}. \quad (33)$$

This is the iteratively reweighted formula. For the absorption compensation problem, $\mathbf{R}^1 = \mathbf{S}$ for the first iteration is used to calculate the $\boldsymbol{\Omega}^k$ in formula 33 and then subsequently substituted again in equation 33 to obtain a new $\mathbf{R}^{k+1}$. The procedure is repeated until the convergence criteria given in equation 34 between successive iterations are met:

$$\frac{\|\mathbf{R}^{k+1} - \mathbf{R}^k\|}{1 + \|\mathbf{R}^{k+1}\|} < \delta, \quad (34)$$

where δ is tolerance.

Two user-defined parameters are now controlling the behavior of the solution of inverse problems: β and ε. A small value of ε can stabilize the objective functional (equation 28), but too small a value

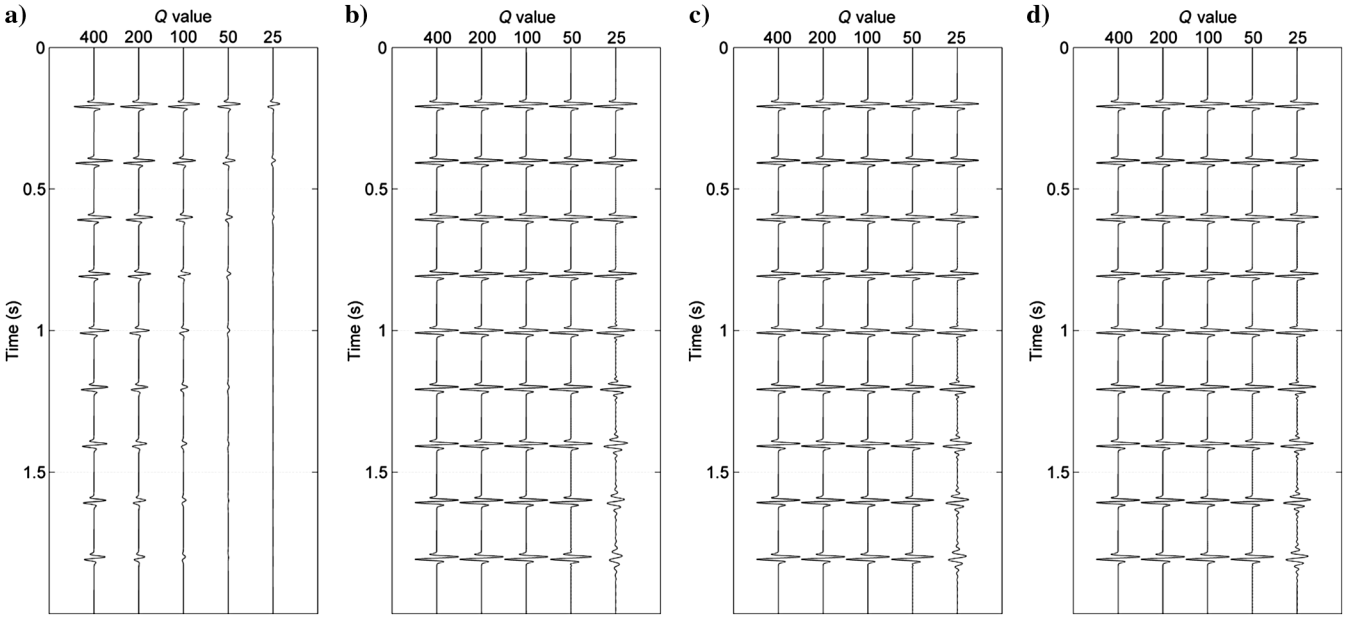

Figure 2. The synthetic seismic record and attenuation compensation results: (a) the synthetic seismic record, (b) the compensation results using zero-order regularization, (c) the compensation results using first-order regularization, and (d) the compensation results using second-order regularization.

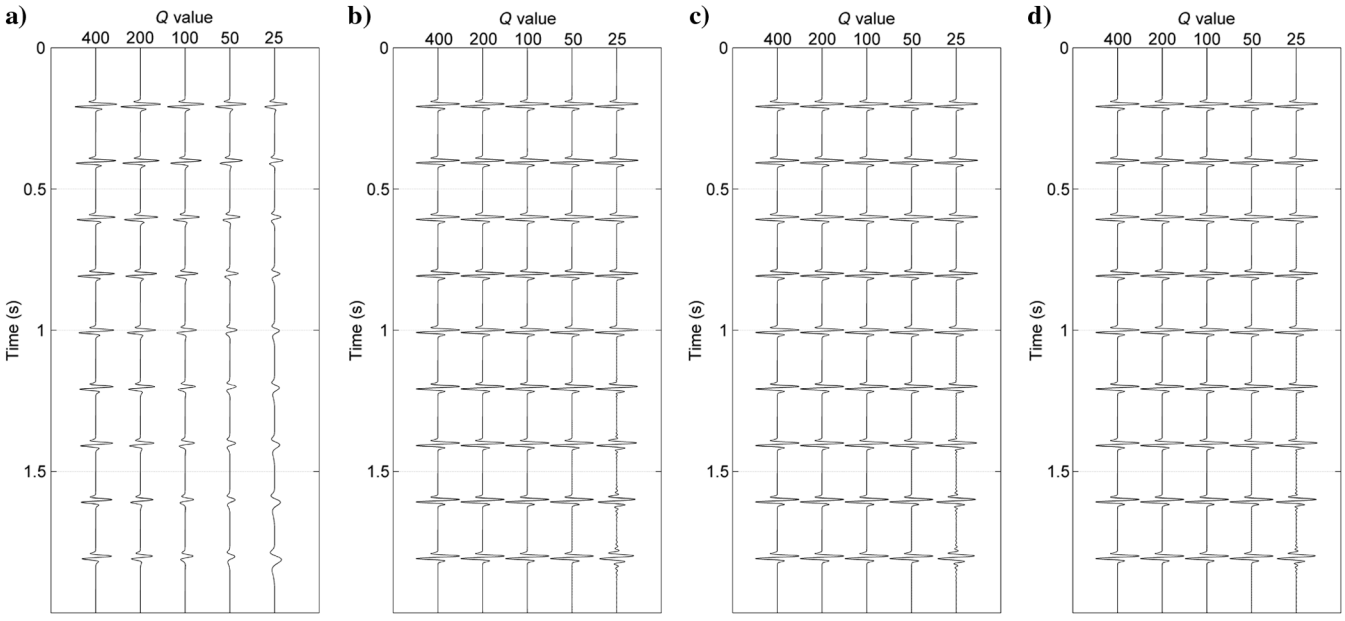

Figure 3. The synthetic seismic record and attenuation compensation results using the weight function: (a) the synthetic seismic record, (b) the compensation results using zero-order regularization, (c) the compensation results using first-order regularization, and (d) the compensation results using second-order regularization.

can introduce instability. On the other hand, too large a value of ε will make $\sum_{i=1}^{n}\sqrt{r_i^2+\varepsilon^2}$ far from the l_1-norm. The regularization parameter β is the trade-off parameter between the residual and model norm. If β is a relatively large number, the noise will be attenuated at the expense of a less accurate approximation of the model. On the other hand, if β is too small, the noise will dominate the out results, which leads to instability in the inversion. Therefore, β is a trade-off between accuracy and instability in the inverse algorithm. If the signal-to-noise ratio (S/N) of the data is high, β can be chosen to be very small. If the S/N of the data is very low, then β should be chosen as relatively large values.

Formula 33 can be used to minimize the functional (equation 28). Figure 5 is the compensation result of Figure 4a using formula 33. From the comparison between Figures 5 and 4b, we can see that the l_1-norm regularization method can recover more high-frequency components.

NOISY DATA EXPERIMENT

To demonstrate the performance of the l_1-norm regularization method, we applied our compensation method to the noisy data. The model is also Figure 1, the dominant frequency of the wavelet is 30 Hz, and the Q value is 25. The synthetic seismic records without noise are shown in Figure 6a. The seismic records with 20% random noise are shown in Figure 6b. Figure 6c is the synthetic records without attenuation. The purpose of attenuation compensation is to recover Figure 6c from 6b. The compensation results using l_2-norm regularization are shown in Figure 6d, and the compensation results using l_1-norm regularization are shown in Figure 6e. Comparing Figure 6d and 6e, we can see that l_1-norm regularization has more strong antinoise ability. Parameters ε and β are two important parameters during processing. The values of ε and β are chosen as 1×10^{-12} and 0.02 in Figure 6e. In general, ε is chosen to be very small and the processing result is not very sensitive to parameter ε. Figure 6f is the compensation results with $\varepsilon = 1\times10^{-10}$ and $\beta = 0.02$, respectively. Figure 6e and 6f is almost the same. Parameter β is chosen according to the S/N of the input trace. In this experiment, the S/N is 5, the l_2-norm of the trace is approximately 0.1, and β is chosen as $0.1/5 = 0.02$.

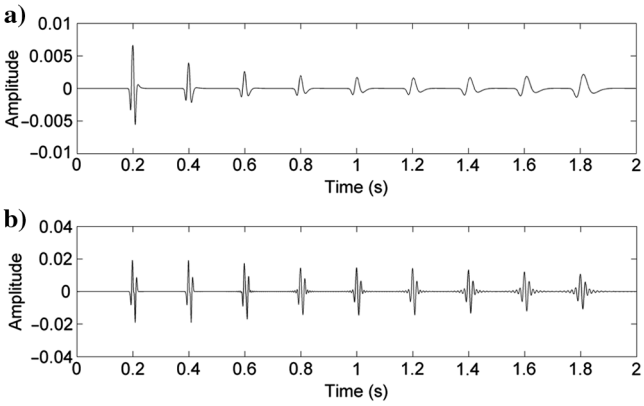

Figure 4. The synthetic seismic record and attenuation compensation results with the wavelet of the dominant frequency, 80 Hz: (a) the synthetic seismic record and (b) the compensation result using second-order regularization.

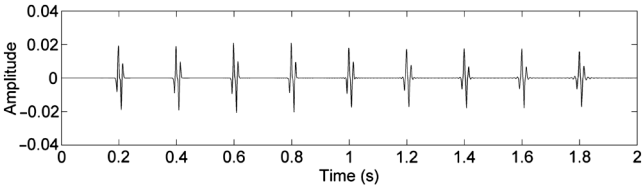

Figure 5. The compensation results using the l_1-norm regularization method.

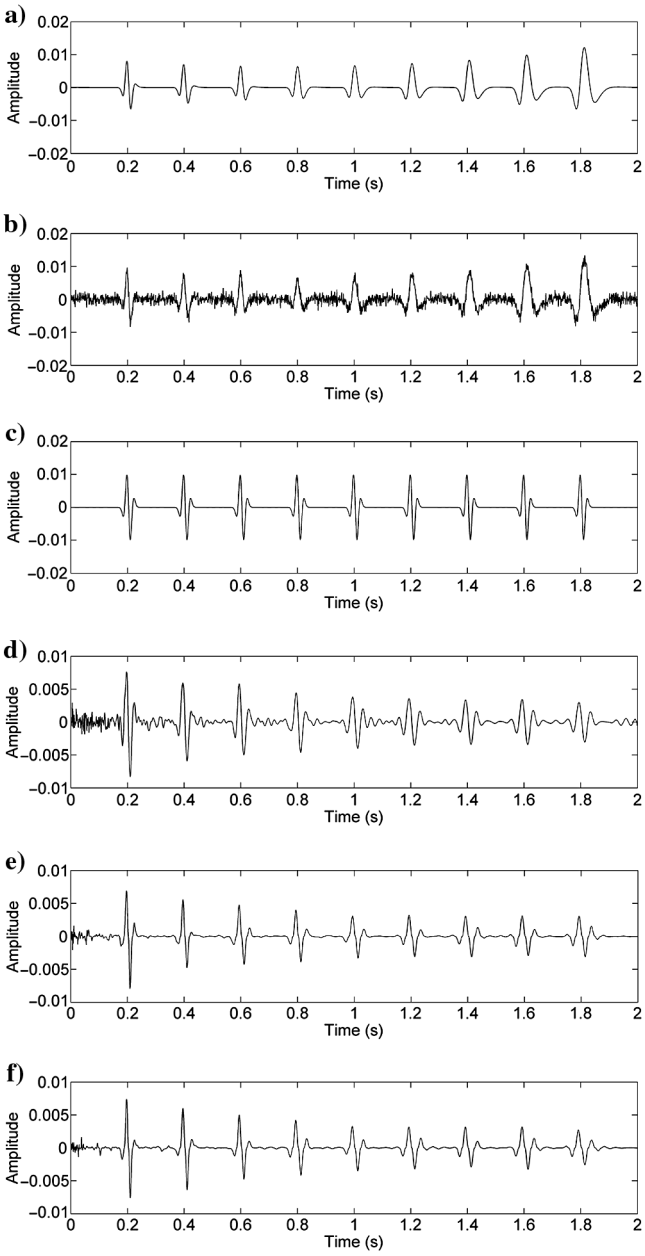

Figure 6. The noisy data experiment. (a) The synthetic seismic records with attenuation. (b) The synthetic seismic records with 20% random noise. (c) The synthetic seismic records without attenuation. (d) The compensation results using the l_2-norm regularization method. (e) The compensation results using the l_1-norm regularization method with $\varepsilon = 1\times10^{-12}$ and $\beta = 0.02$. (f) The compensation results using the l_1-norm regularization method with $\varepsilon = 1\times10^{-10}$ and $\beta = 0.02$.

REAL DATA EXPERIMENT

Figure 7 shows a seismic section of marine seismic reflection data after migration. The l_1-norm regularization method is used to process the data. Quality factor $Q = 120$ is set through a series of tests. The results of compensation are shown in Figure 8. Parameters ε and β are chosen as 1×10^{-10} and 0.1. Comparing these two sections, we can see that the resolution of the migration section is improved. Several reflections that are not separated in the section shown in Figure 6 can be observed after compensation, and the lateral continuity can be tracked from trace to trace. To demonstrate the details of the compensation, we show the single trace contrast. Figure 9a shows the original seismic trace at the CDP = 15,600 position, and Figure 9b shows the trace after compensation. Figure 9c is the fitting residual, that is, **AWR − AS** in equation 27. We can see that the residual is very small and mainly random noise. Figure 10 shows the amplitude spectrum before and after compensation. Figure 10a is the amplitude spectrum corresponding to Figure 9a, and Figure 10b is that corresponding to Figure 9b. The maximum magnitude spectral component of the original data is about 100 Hz and is unchanged. After compensation, higher frequencies are boosted. Figure 10 illustrates that the compensation broadens the spectrum and the high-frequency component is compensated reasonably.

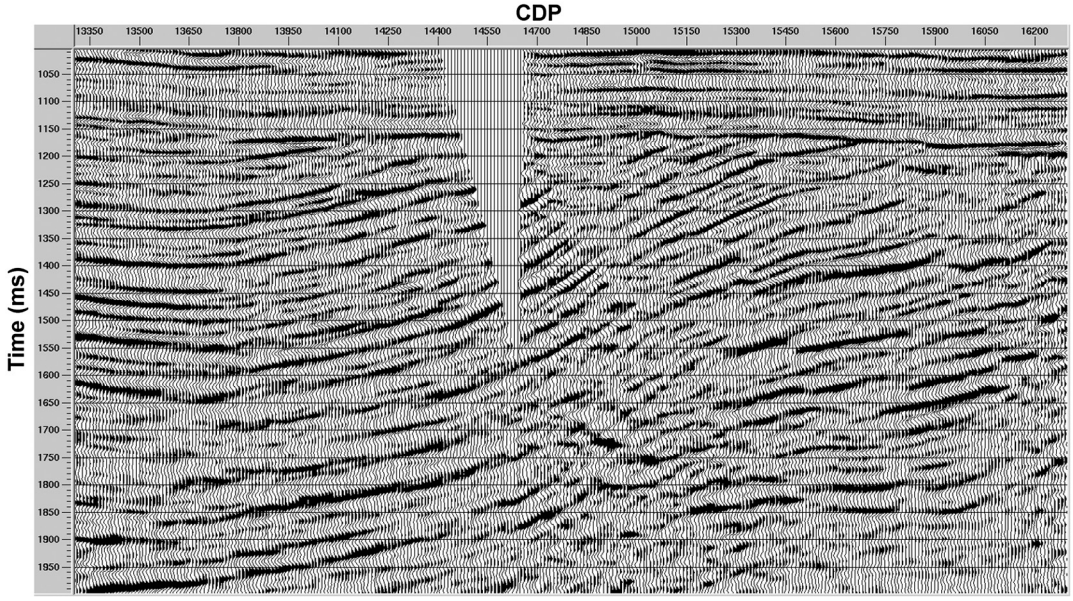

Figure 7. A migrated seismic section of marine seismic reflection data.

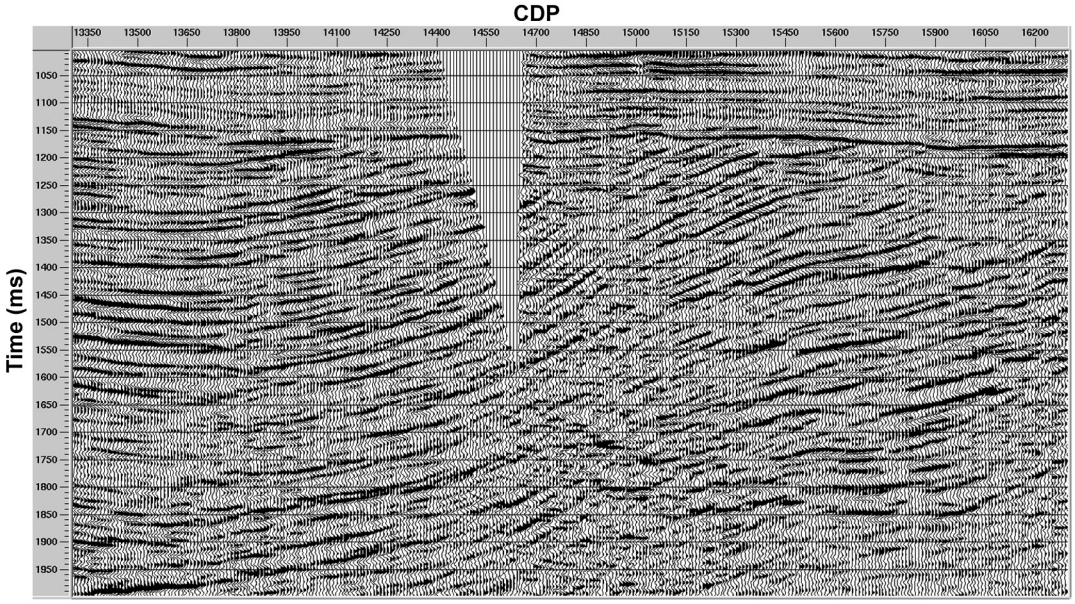

Figure 8. The seismic section after attenuation compensation.

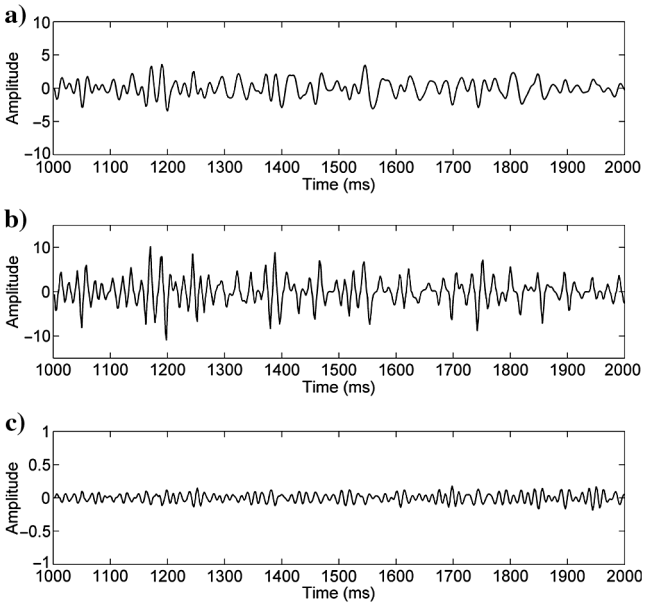

Figure 9. Single trace comparison. (a) The original seismic trace. (b) The seismic trace after attenuation compensation. (c) Fitting residual data.

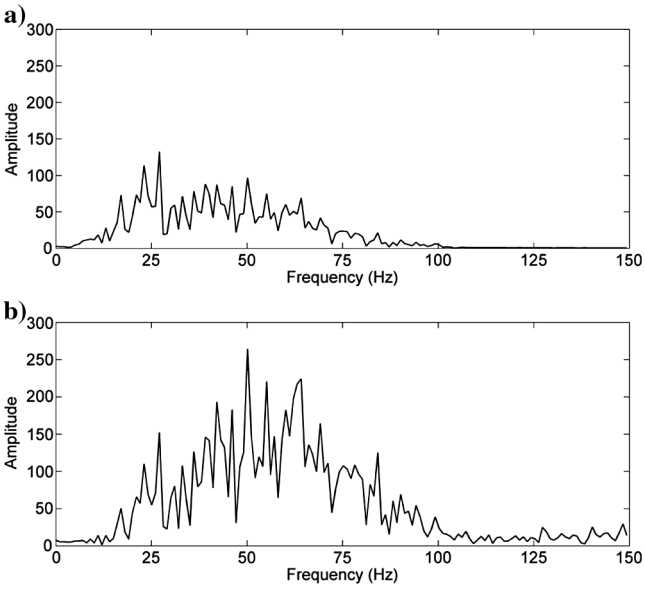

Figure 10. The spectrum comparison of single trace. (a) The amplitude spectrum of original trace. (b) The amplitude spectrum after attenuation compensation.

CONCLUSIONS

Attenuation compensation is an important method for improving the resolution of seismic data. The attenuation compensation problem can be reduced to solving the problem of the Fredholm integral equation in the time domain. For the problem that the shallow and deep data are not equally weighted in the objective functional, the weight function method can be used to improve the computational accuracy. An attenuation compensation method based on l_1-norm regularization is proposed in this paper. For seismic data with high dominant frequency, the l_1-norm regularization method can obtain better compensation results than can l_2-norm regularization. For seismic data with noise, the l_1-norm regularization method is more robust than is l_2-norm regularization. The synthetic and real data results demonstrate that the l_1-norm regularization attenuation compensation method presented in this paper is stable and accurate.

ACKNOWLEDGMENTS

The authors appreciate the support of the National Natural Science Foundation of China (41274137) and the National Science and Technology Major Project of China (2011ZX05023-005-005).

REFERENCES

Azimi, S. A., V. V. Kalinin, and B. L. Pivovarov, 1968, Impulse and transient characteristics of media with linear and quadratic absorption laws: Izvestiya, Physics of the Solid Earth, **2**, 88–93.

Baan, M. V., 2012, Bandwidth enhancement: Inverse Q filtering or time-varying Wiener deconvolution?: Geophysics, **77**, no. 4, V133–V142, doi: 10.1190/geo2011-0500.1.

Bickel, S. H., 1993, Similarity and the inverse Q filter: The Pareto-Levy stretch: Geophysics, **58**, 1629–1633, doi: 10.1190/1.1443378.

Bickel, S. H., and R. R. Natarajan, 1985, Plane-wave Q deconvolution: Geophysics, **50**, 1426–1439, doi: 10.1190/1.1442011.

Farquharson, C. G., and D. W. Oldenburg, 1998, Non-linear inversion using general measures of data misfit and model structure: Geophysical Journal International, **134**, 213–227, doi: 10.1046/j.1365-246x.1998.00555.x.

Futterman, W. I., 1962, Dispersive body waves: Journal of Geophysical Research, **67**, 5279–5291, doi: 10.1029/JZ067i013p05279.

Hargreaves, N. D., 1992, Similarity and the inverse Q filter: Some simple algorithms for inverse Q filtering: Geophysics, **57**, 944–947, doi: 10.1190/1.1443307.

Hargreaves, N. D., and A. J. Calvert, 1991, Inverse Q filtering by Fourier transform: Geophysics, **56**, 519–527, doi: 10.1190/1.1443067.

Innanen, K. A., and J. E. Lira, 2010, Direct nonlinear Q-compensation of seismic primaries reflecting from a stratified, two-parameter absorptive medium: Geophysics, **75**, no. 2, V13–V23, doi: 10.1190/1.3337695.

Kjartansson, E., 1979, Constant Q-wave propagation and attenuation: Journal of Geophysical Research, **84**, 4737–4748, doi: 10.1029/JB084iB09p04737.

Margrave, G. F., M. P. Lamoureux, and D. C. Henley, 2011, Gabor deconvolution: Estimating reflectivity by nonstationary deconvolution of seismic data: Geophysics, **76**, no. 3, W15–W30, doi: 10.1190/1.3560167.

Mittet, R., 2007, A simple design procedure for depth extrapolation operators that compensate for absorption and dispersion: Geophysics, **72**, no. 2, S105–S112, doi: 10.1190/1.2431637.

Mittet, R., R. Sollie, and K. Hokstad, 1995, Prestack depth migration with compensation for absorption and dispersion: Geophysics, **60**, 1485–1494, doi: 10.1190/1.1443882.

Qaji, W. O., and A. Rietbrock, 2011, Enhanced seismic Q compensation: 81st Annual International Meeting, SEG, Expanded Abstracts, 2737–2741.

Shou-Dong, W., 2011, Attenuation compensation method based on inversion: Applied Geophysics, **8**, 150–157, doi: 10.1007/s11770-011-0275-3.

Song, S., and K. Innanen, 2002, Multiresolution modeling and seismic wavefield reconstruction in attenuating media: Geophysics, **67**, 1192–1201, doi: 10.1190/1.1500381.

Toverud, T., and B. Ursin, 2005, Comparison of seismic attenuation models using zero-offset vertical seismic profiling (VSP) data: Geophysics, **70**, no. 2, F17–F25, doi: 10.1190/1.1884827.

Varela, C. L., A. L. R. Rosa, and T. J. Ulrych, 1993, Modeling of attenuation and dispersion: Geophysics, **58**, 1167–1173, doi: 10.1190/1.1443500.

Wang, Y., 2002, A stable and efficient approach of inverse Q filtering: Geophysics, **67**, 657–663, doi: 10.1190/1.1468627.

Wang, Y., 2003, Quantifying the effectiveness of stabilized inverse Q filtering: Geophysics, **68**, 337–345, doi: 10.1190/1.1543219.

Wang, Y., 2006, Inverse Q-filter for seismic resolution enhancement: Geophysics, **71**, no. 3, V51–V60, doi: 10.1190/1.2192912.

Zhang, C., and T. J. Ulrych, 2007, Seismic absorption compensation: A least squares inverse scheme: Geophysics, **72**, no. 6, R109–R114, doi: 10.1190/1.2766467.